Journal of Power Sources 220 (2012) 95–102

Contents lists available at SciVerse ScienceDirect

Journal of Power Sources

journal homepage: www.elsevier.com/locate/jpowsour

Two kinds of graphene-based composites for photoanode applying in dye-sensitized solar cell

Bo Tang, Guoxin Hu*

School of Mechanical and Power Engineering, Shanghai Jiaotong University, No. 800 Dongchuan Road, Shanghai 200240, China

HIGHLIGHTS

- A novel photoanode with three-layer structure is prepared for DSSCs.
- The η reaches 8.67% when the prepared photoanode is adopted.
- Scattering and transport layers obviously increase the J_{sc} and V_{oc}.
- The detailed characterizations of the adding layers are performed.

GRAPHICAL ABSTRACT

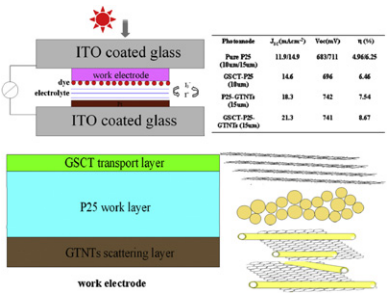

ARTICLE INFO

Article history:
Received 18 June 2012
Received in revised form
23 July 2012
Accepted 26 July 2012
Available online 7 August 2012

Keywords:
Graphene
Scattering layer
Transport layer
Photoanode

ABSTRACT

Two kinds of graphene modified TiO_2 composites are synthesized by hydrothermal method and layer-by-layer self-assembly technology. Graphene/titanate nanotubes (GTNTs) films have great light-harvesting efficiencies, and the amount of graphene does not obviously influence their optical performance. Alternating graphene/TiO_2 (prepared by supercritical treatment, GSCT) multilayer films possess superior electron transport ability, and the number of bi-layers plays as a central role for their electrical property. The outstanding light scattering and carrier transport properties of these promising films promote the performance of dye-sensitized solar cells (DSSCs). The power conversion efficiencies (η) of the DSSCs reach 6.46% and 7.54% under AM-1.5G by using GSCT-P25 (10 μm) and P25-GTNTs (15 μm) photoanodes, and the increases are 33.8% and 20.6% compared with that of by using a P25 photoanode with same thickness. The η reaches 8.67% when a preliminarily optimized GSCT-P25-GTNTs (15 μm) photoanode is adopted, which is far better than employing a pure P25 photoanode (6.25%).

1. Introduction

The increased demand for energy consumption has continued to put pressure on the whole human society. With the depletion of fossil fuels, more attention has been paid to the development of renewable-energy in the past decades. There into, solar energy has been regarded as a potential candidate because of it is free and inexhaustible. Dye-sensitized solar cells (DSSCs) have attracted intense interest after the groundbreaking report in 1991 [1]. Gratzel et al. adopted nano-scaled TiO_2 as photoanode for the first time and obtained a power conversion efficiency (η) as high as 7%. Recently, various attempts have been made to improve the efficiency of DSSCs. The major works were focused on two directions: fabricating more efficient dyes and improving performance of electrodes [2–16]. Gratzel groups prepared a series of dyes based on Ru complexes. N3 dye possesses high incident photon-to-current conversion efficiency (IPCE) in a wide wavelength range (the η as high as 10%) [2]. Moreover, the "black dye" (N749) extends the high IPCE to 920 nm (η up to 10.4%) [3]. Due to the high-cost of Ru complexes, some new dyes including indoline, porphyrin and

* Corresponding author. Tel./fax: +86 21 34206569.
E-mail address: hugx@sjtu.edu.cn (G. Hu).

0378-7753/$ – see front matter © 2012 Elsevier B.V. All rights reserved.
http://dx.doi.org/10.1016/j.jpowsour.2012.07.093

phthalocyanine have been fabricated in recent years [4–8]. Horiuchi et al. reported the fabrication of indoline dye, and the resulted η reached 6.1% [4]. Nazeeruddin et al. researched the features of Zn-porphyrin dyes [9]. Overall, outstanding properties of the above-mentioned dyes are able to meet the requirements, which is ahead of the development of other parts of the DSSCs.

Except the development of new dyes, improving the performance of photoanode is another method to promote the η of the DSSCs. Lin et al. reported a novel ZnO photoanode, and a high conversion efficiency 6.06% was achieved (thickness of the photoanode is 15 μm) [10]. Kamat et al. prepared single walled carbon nanotube (SWCNT) assisted TiO_2 photoanode [11]. Due to the enhanced charge transport ability, marked improvement in the IPCE and η were gained. Wang et al. fabricated shell-in-shell TiO_2 hollow spheres modified electrode, and the η was significantly increased due to its high light-harvesting efficiency [13]. Most recently, graphene modified DSSCs were anticipated to obtain higher conversion efficiency [17]. Mullen et al. adopted graphene as the transparent electrode substrate to replace the indium tin oxide, which opened the door for the applications of graphene in the DSSCs field [18]. Apart from be used as the conductive substrate, graphene can also be mixed with TiO_2 to play as the photoanode. Gao et al. found that the η increased 59% after adding graphene in the photoanode (η reached 4.28%) [19]. Although several papers have been reported, there is still large space to further boost the performance of graphene assisted DSSCs.

In this study, we report a novel photoanode with three-layer structure. The inner layer consists of alternant graphene and TiO_2 (GSCT), which provides the fast electron transport channel between P25 and conductive glass. The middle P25 layer acts as the work layer to produce electron–hole pairs. The outer layer is graphene modified titanate nanotubes (GTNTs) film. Its excellent scattering property enhances the light-absorption efficiency of the work layer. Based on the above description, the GSCT and GTNTs films are designated as transport and scattering layers, respectively. The GTNTs paste was fabricated by the hydrothermal method with chemical reduced graphene and P25 as starting materials. Layer-by-layer (LBL) self-assembly technology was used to prepare the GSCT film, and the adopted TiO_2 (SCT) was preconfigured by the supercritical measurement. After adding to the photoanode, these two films significantly increased the η of the DSSCs. The influence on the η from graphene content in the scattering layer was studied, and the transport layers with varied numbers of bi-layers were also prepared to optimize the photoanode. After preliminary optimization, the η as high as 6.46%, 7.54% and 8.67% were achieved by using the GSCT-P25 (10 μm), P25-GTNTs (15 μm) and GSCT-P25-GTNTs (15 μm) photoanodes based DSSCs, respectively (the η were 4.96% and 6.25% by using 10 μm and 15 μm pure P25 photoanode based samples, respectively).

2. Experimental section

2.1. Reagents and materials

Natural graphite was obtained from Alfa Aesar Co. P25 was purchased from Degussa. Nanoscale TiO_2 (anatase type) was obtained from Shanghai Jianghu industrial Co., Ltd. Acetonitrile, polytetrafluoroethylene and sodium dodecyl sulfate (SDS) were obtained commercially from the Beijing chemical reagent plant (Beijing, China). Polyethyleneimine (PEI) aqueous solution, chloroplatinic acid, indoline, iodine and potassium iodide were purchased from Aladdin Co. Deionized water (resistivity 18 MΩcm) was utilized to prepare all aqueous solutions. The P25 and nanoscale TiO_2 were sintered at 500 °C for 2 h to remove organics and dust for the subsequent experiments.

2.2. Preparation of additional films

2.2.1. GTNTs

Synthesis process of the GTNTs is shown as Scheme 1a, and the details (including fabricating pure TNTs) are according to our recent work [20].

2.2.2. Preparation of GSCT

25 mg as-prepared pure TNTs powder was added to 10 mL deionized water and followed by supersonic treatment for 15 min. Afterwards, the mixture was carefully moved to a sealed reactor (a pressure-resistant SCHOELLER 316L SS vessel with 15 cm^3 volume) and then heated to 400 °C (keeping 2 h) for supercritical reaction. After reaction, the reactor was rapidly cooled in the ice bath. The as-prepared SCT was treated with ultrasonic for 5 min. Modified Hummers' method was used to prepare graphene oxide first, and then hydrazine was adopted to achieve the reduction of the graphene oxide in 98 °C water bath for 6 h. In order to obtain a well-dispersed high quality graphene solution, lysozyme was added and pH value was adjusted to 10 (more details see supplementary data) [21]. The beforehand chemical reduced graphene and SCT were handled by LBL self-assembly technology to

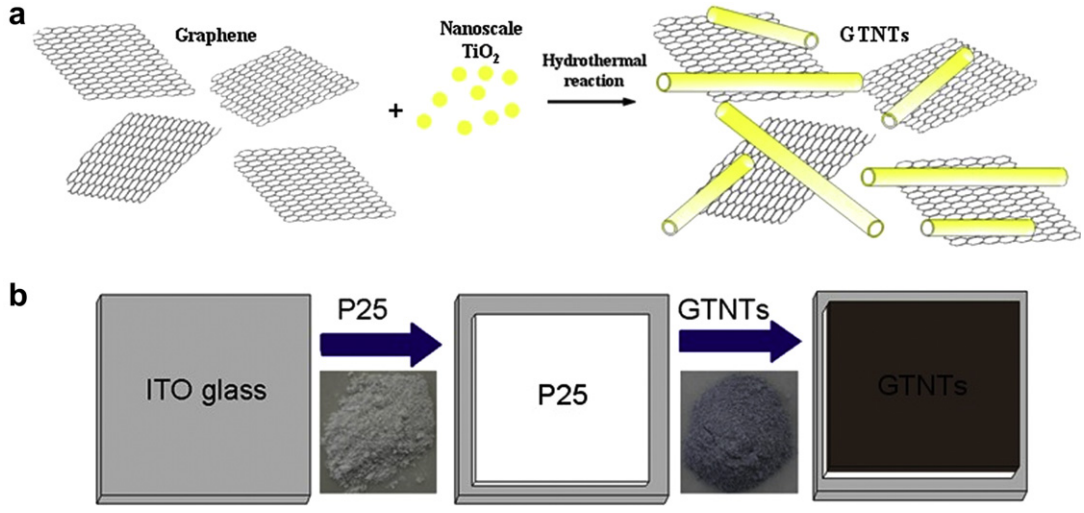

Scheme 1. The form process of the GTNTs (a) and the P25-GTNTs photoanode (b).

fabricate the GSCT. Briefly, a conductive glass (coating ITO) was immersed into a protonic PEI aqueous solution for 15 min to introduce positive charges, and followed by washing with deionized water for 2 times (step 1). Afterwards, the conductive glass was immersed into a colloidal suspension of the SCT for 15 min and then washed for 2 times (step 2). After that, the sample was immersed into the PEI solution for 15 min and rinsed for 2 times (step 3). The resulted sample was immersed into a graphene nanosheets solution for 15 min and washed for 2 times (step 4). The steps 1–4 were repeated until the desired number of bi-layer was obtained (see Scheme 2). Subsequently, the prepared films were illuminated under UV-light for 24 h to remove the PEI. In this study, 2, 5, 10, 20 and 50 bi-layers films were prepared.

2.3. Preparation of photoanodes

2.3.1. P25 photoanode

The conductive glass was cleaned by propanol with an ultrasonic bath for 1 h and then rinsed with deionized water. The P25 film was deposited on the conductive glass by doctor-blade method, and the prepared sample was heated to 300 °C and kept 30 min.

2.3.2. GSCT-P25 photoanode

The fabrication process is similar with the P25 photoanode except that the GSCT was pre-prepared on the surface of the conductive glass.

2.3.3. P25-GTNTs photoanode

The prepared GTNTs was mixed with polytetrafluoroethylene (4 wt%) and then deposited on the surface of P25 photoanode by doctor-blade method. The synthesis processes of the P25-GTNTs photoanode are shown as Scheme 1b.

2.3.4. GSCT-P25-GTNTs photoanode

The prepared GTNTs paste was deposited on the surface of beforehand GSCT-P25 photoanode by doctor-blade method.

2.4. Preparation of Pt electrode

0.1 g chloroplatinic acid was added to 10 mL propyl alcohol solution, and then the solution was dropped to the surface of a clear conductive glass for several times. After air dry, the specimen was heated to 380 °C and kept for 15 min to fabricate the Pt electrode.

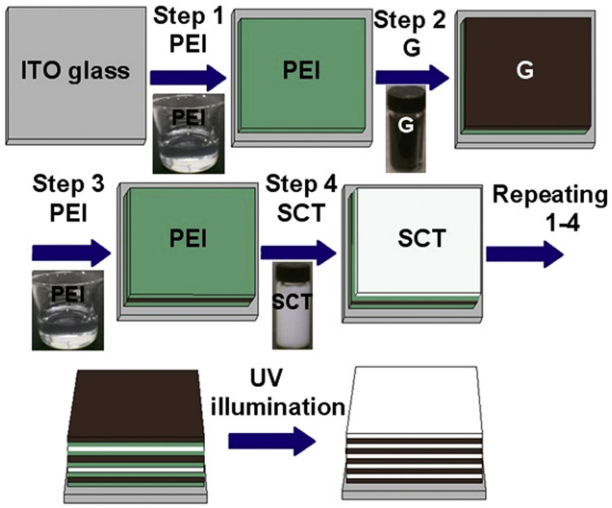

Scheme 2. The preparation process of the GSCT.

2.5. Characterization

X-ray diffraction (XRD) analysis was recorded on Bruker D8 Advance using Cu Kα radiation (λ = 0.154 nm). X-ray photoelectron spectroscopy (XPS) was measured on an RBD upgraded PHI-5000C ESCA system (Perkin Elmer). The morphology images of prepared samples were carried out by transmission electron microscopy (TEM) (JEM-2100F operated at an accelerating voltage of 20 kv). Raman spectra were performed by LabRam-1B Raman microspectrometer at 514.5 nm (Horiba Jobin Yvon, France). The Brunauer–Emmett–Teller (BET) surface areas of the photocatalysts were measured on a Nova 100 by using N_2 as the adsorption gas. Atomic Force Microscopy (AFM) results were recorded by Nanoscope IIIa (Digital Instrument, USA) and E-Sweep (Seiko, Japan) in tapping mode. Scanning electron microscope (SEM) images were obtained by FEI Sirion 200 scanning electron microscope working at 5 kV. UV–visible diffuse reflectance spectra were carried out on a TU-1901 UV–visible spectrophotometer. Fourier transform infrared (FTIR) spectra were recorded by an IR Prestige-21 system (PerkinElmer) with KBr as the reference sample. Photocurrent measurements and electrochemical impedance spectroscopy (EIS) were performed on a CHI 660D electrochemical analyzer (Shanghai CH Instrument Company, China).

2.6. Preparation and measurement of DSSCs

The as-prepared P25, GSCT-P25, P25-GTNTs and GSCT-P25-GTNTs photoanodes were immersed into 0.5 mmol indoline dye solution with a 1:1 (volume) mixture of acetonitrile and butanol and kept for 30 h. These photoanodes and Pt electrodes were assembled into sandwich type cells and sealed with surlyn films. The electrolyte including acetonitrile solution, 0.5 mol LiI and 0.05 mol I_2 was introduced between the electrodes. The schematic structure and energy diagram of the prepared DSSCs are shown in Scheme 3. The *J–V* curves were recorded by a PGSTAT 30

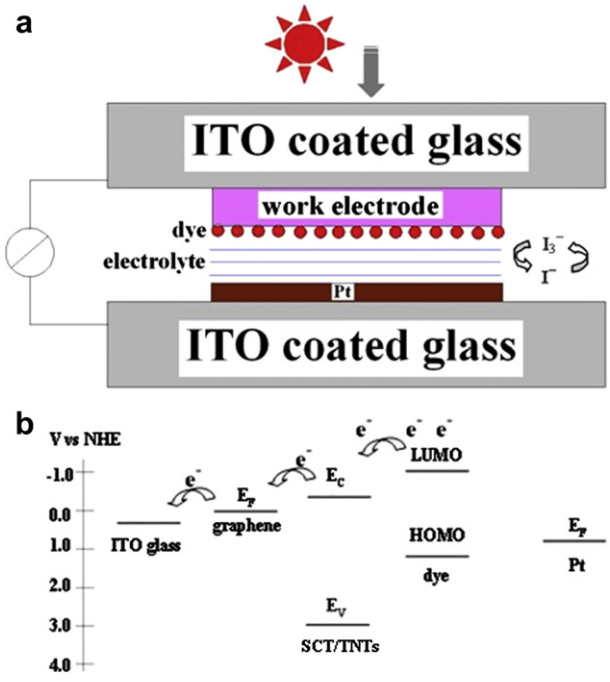

Scheme 3. The schematic structure (a) and energy diagram (b) of the GSCT-P25-GTNTs photoanodes based DSSCs.

potentiostat (Netherlands). The IPCE profiles were recorded on a Newport 1918-c power meter.

3. Results and discussion

3.1. Characterization of the GSCT and GTNTs

TEM images of the as-prepared pure TNTs and SCT are shown in Fig. 1. Before supercritical reaction, the tubular TNTs with 7∼9 nm in diameter and several hundred nanometers in length can be seen from Fig. 1a, and the high magnification TEM image clearly shows a strong contrast between the dark wall and pale center (see the inset). Fig. 1b shows typical morphology of the as-prepared SCT (including TiO_2 nanoparticles and monolayer TiO_2 with rhombic appearance), indicating that the tubular TNTs were opened after the supercritical treatment. Typical thickness of the SCT is about 0.4∼2 nm from the AFM image (inset of Fig. 1c), demonstrating the presence of both monolayer TiO_2 and TiO_2 nanoparticle [22,23]. In fact, the proportion between them can be controlled by adjusting the reaction conditions, which is beyond the scope of this paper.

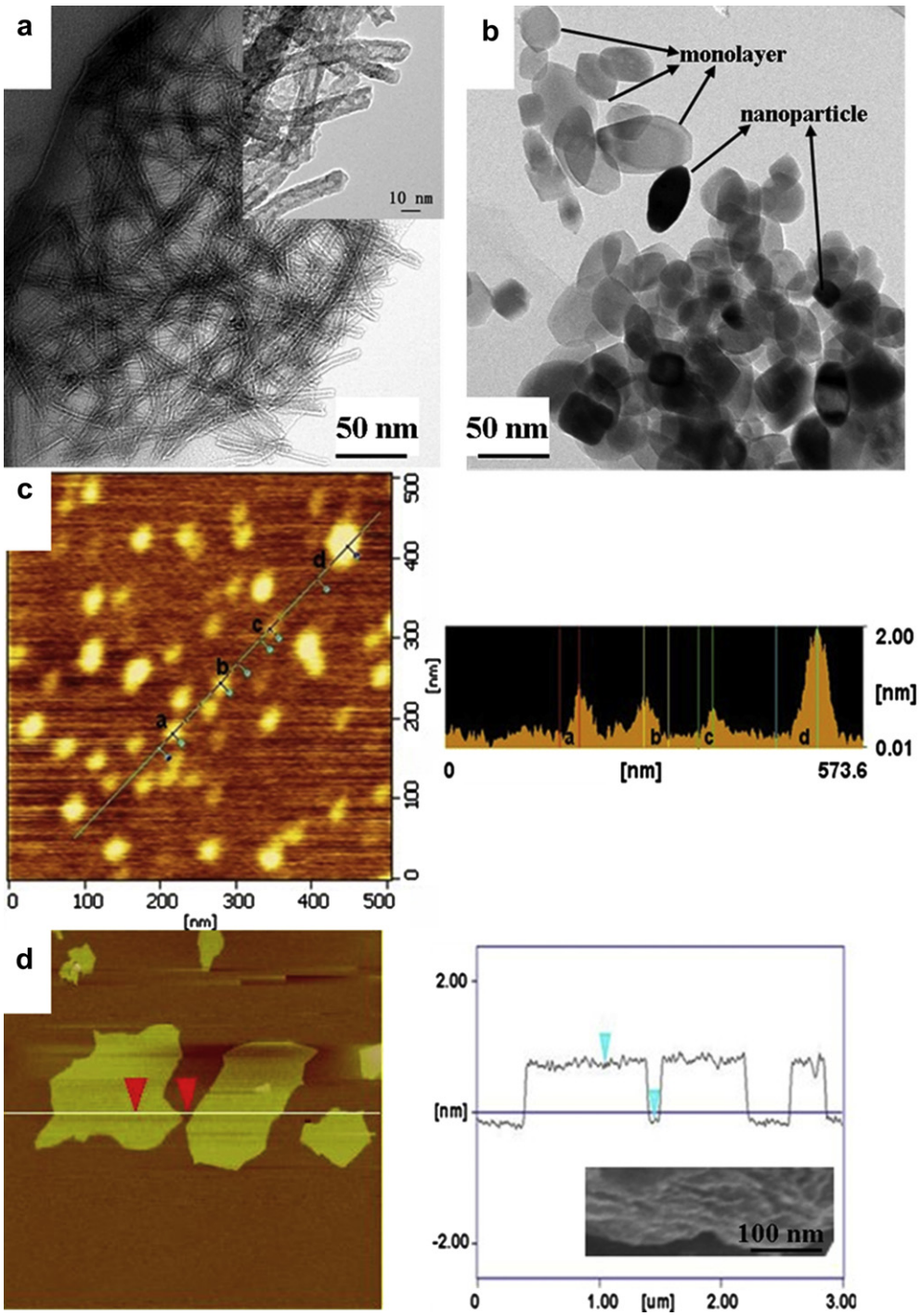

Fig. 1. (a) TEM images of the pure TNTs, the inset shows the high magnification image; (b) TEM image of the SCT, monolayer TiO_2 and TiO_2 nanoparticle are marked; (c) AFM images of the SCT; (d) AFM images of the graphene, inset shows the cross-sectional SEM image of the GSCT (50 bi-layers).

Moreover, AFM image reveals the monolayer feature of the prepared graphene (typical thickness about 0.6 nm of the chemical reduced graphene is shown in Fig. 1d) [24]. The cross-sectional SEM images unambiguously display the multilayer structure of the GSCT (50 bi-layers), demonstrating the efficient combination of the graphene and SCT (inset of Fig. 1d). In theory, the loosened structure is good for dye absorption and ion transport, which can promote the performance of the photoanode.

In order to further confirm the combination of the graphene and SCT, XPS was used to analyze the SCT and GSCT (10 bi-layers). An added peak corresponding to C element appears in the curve of the GSCT only (see supplementary information Fig. S1a). For the Raman spectrum of the SCT and GSCT, the G and D peaks resulting from graphene can also be seen from the GSCT (see supplementary data Fig. S1b). Thereby, both the results of XPS and Raman spectra manifest the successful integration of graphene and SCT [25]. Moreover, the element analysis result of the GSCT (10 bi-layer) is consistent with this point (Fig. S1c). Photocurrent measurements of the GSCT with varied thicknesses were performed to further monitor the consecutive build-up of the graphene and SCT. As shown in Fig. 2, the photocurrent increases with the increased thickness, suggesting the efficient construction of the alternant bi-layers by using LBL self-assembly technology. Therefore, the photoconductivity of the GSCT can be controlled by changing the film thickness, which is similar with the recent report [12]. Furthermore, the fast and uniform photocurrents that observed from all samples reflect the great light response and excellent electrical property of the as-prepared GSCT films.

FTIR was carried out to analyze the graphene, SCT, GSCT and GTNTs (see supplementary data Fig. S1d). In these curves, the low-frequency absorption (<1000 cm^{-1}) is assigned to the Ti—O—Ti vibration, while the broad absorption band from 3000 to 3700 cm^{-1} is attributed to the O—H stretching vibration of hydroxyl from the surface adsorbed water [26]. Compared to that of the pure SCT, a new absorption band resulting from skeletal vibration of the graphene sheets can be seen in the GSCT and GTNTs (around 1600 cm^{-1}). After careful observation the patterns of the GSCT and GTNTs, obvious distinction of the low-frequency region implies the different interaction between the graphene-SCT and graphene-TNTs. The similar profile in the low-frequency range of the SCT and GSCT suggests physical interaction between the graphene and SCT (LBL self-assembly process is based on electrostatic force in this case), while the broadening peak of the GTNTs indicates the formation of chemical bond between the graphene and TNTs during the hydrothermal reaction [20].

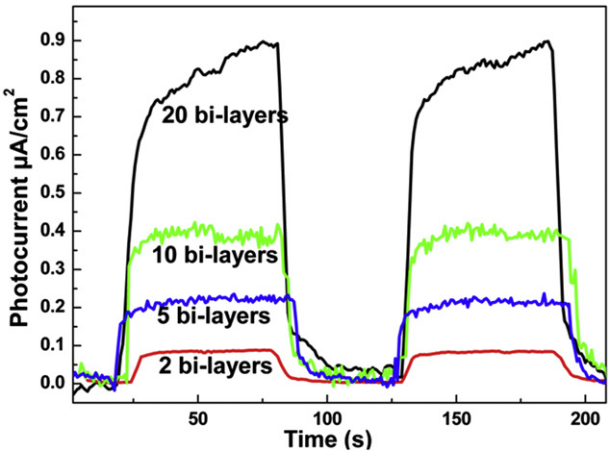

Fig. 2. Photocurrents of the GSCT with varied numbers of bi-layers.

XRD patterns of the GSCT (20 bi-layers) before and after UV-light illumination are shown in Fig. 3. An obvious peak located at 3.82° can be seen in the curve a, proving the periodic layered structure of the GSCT film. The layer spacing was calculated as 2.31 nm based on the Bragg's law. After irradiation under UV-light for 24 h, the diffraction peak shifts to 4.28° due to the remove of PEI (curve b). The layer spacing reduces to 2.16 nm, which is in according with the AFM results (0.6 nm for graphene and nanometer size for SCT). The inset shows XRD curves of the starting materials including the graphene, SCT and TNTs. Due to the long-range order was damaged during the reduction process, only a broad peak centered at 26.5° can be seen for the graphene (more details see supporting information and Fig. S2) [27]. As for the curve of the SCT colloidal suspensions, a rather broad diffraction halo ranging from 20° to 50° appears. It is the characteristic peak of the monolayer TiO_2 in aqueous solution [28]. In addition, some obvious peaks belonging to anatase TiO_2 can be seen, demonstrating that the SCT is composed of monolayer TiO_2 and anatase TiO_2 nanoparticles again. Compared to that of pure TNTs, the absence of diffraction peak around 10° indicates the open of the tubular material, which is consistent with the TEM images.

The detailed characterizations including XPS, XRD, FTIR, UV—vis diffuse reflectance spectra of the GTNTs have been done in elsewhere [20].

3.2. Application of DSSCs

Photovoltaic characteristics of the DSSCs with P25 and GSCT-P25 photoanodes are summarized in Table 1. Compared to that of the pristine P25 photoanode based DSSCs, all the GSCT assisted samples (the thicknesses of these photoanodes are identical: 10 μm) exhibit an obvious increase in short-circuit current density (J_{sc}). The increased amounts of the J_{sc} reach 16.8%, 22.7% and 24.3% by using GSCT (5 bi-layers)-P25, GSCT (10 bi-layers)-P25 and GSCT (20 bi-layers)-P25 photoanodes, respectively. Three possible reasons may lead to the improved J_{sc} in this case: (1) more dye molecules are adsorbed in the photoanode, which will promote the generation of photogenerated electrons. (2) More efficient electron transport from P25 to conductive glass is achieved. (3) Enhanced light-to-electron conversion efficiency is obtained by adding a light scattering layer. The dye adsorption amounts of these photoanodes are listed in Table 1, and the presence of the GSCT film does not increase the amount. Although the lamellar and loosened structure

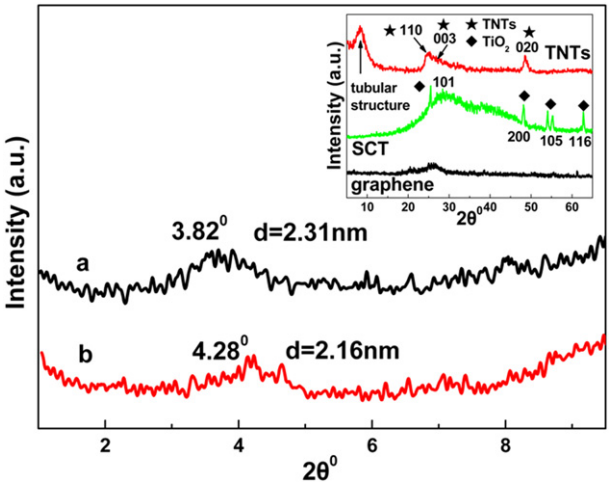

Fig. 3. XRD profiles of the GSCT before (curve a) and after (curve b) UV-light illumination, the inset shows XRD curves of the pre-prepared graphene, TNTs and SCT.

Table 1
Results of photovoltaic properties and dye loading of the DSSCs with varied photoanodes. All measurements were recorded under AM-1.5G one sun and the active areas were ca. 0.15 cm^2 for all cells. Moreover, the BET areas of the P25, TNTs and all GTNTs were also summarized.

Photoanodes	J_{SC} ($mAcm^{-2}$)	V_{oc} (mV)	FF (%)	η (%)	Thickness (μm)	Absorbed dye ($\times 10^{-7}$ $molcm^{-2}$)	BET area (m^3g^{-1})
Pure P25	11.9	683	61.0	4.96	10.0	0.87	49.757
5-GSCT-P25	13.9	694	63.4	6.12	10.1	0.86	–
10-GSCT-P25	14.6	696	63.6	6.46	10.2	0.84	–
20-GSCT-P25	14.8	689	63.4	6.49	10.0	0.89	–
Pure P25	14.9	711	59.0	6.25	15.1	1.29	49.757
P25-GTNTs-0%	16.9	744	57.5	7.23	10.1+5	1.47	276.574[20]
P25-GTNTs-1%	18.3	742	55.6	7.54	10.0+5	1.41	292.107[20]
P25-GTNTs-5%	18.1	756	53.6	7.33	10.0+5	1.59	330.267[20]
P25-GTNTs-10%	17.5	749	52.8	6.92	10.2+5	1.43	301.612[20]

of the GSCT film is good for dye absorption, the thickness of the prepared GSCT films is too small. Compared to that of work layer (P25), thickness of the GSCT films can be ignored (thickness of 20 bi-layers GSCT is about ∼44 nm, while the thickness of the P25 layer is 10 μm). Based on the identical reason, the added GSCT film cannot enhance the light-harvesting efficiency of the photoanode. Moreover, the GSCT film is sandwiched between the P25 film and conductive glass, indicating that the additional film cannot play as a light scattering layer (contrarily, a fraction of incident light is diffused and absorbed by the GSCT film) [29]. The similar reflectivity of the P25 and GSCT-P25 photoanodes unambiguously verifies this view (Fig. 4a).

Therefore, the reasonable explanation for the enhanced J_{sc} is the improved charge transport efficiency. As we know, the excellent electron mobility of graphene makes it a promising material as electron transport channel [30,31]. Furthermore, the Fermi level of graphene is more positive than the conduction band energy of TiO_2 (0 VvsNHE for graphene and −0.5 VvsNHE for TNTs) [32–34]. The photogenerated electrons in the P25 tend to inject into graphene and then transfer to conductive glass quickly (see Scheme 3b), while holes stay on the valence band of TiO_2. Thereby, the recombination of electron–hole pairs in the work layer is suppressed by adding the GSCT film, as well. At the beginning, the J_{sc} and η increase with the increased thickness of the GSCT film. With the saturation of electron transport channel (the amount of photogenerated electrons is a definite value for the P25 photoanode with a certain thickness), the further incremental thickness of the GSCT does not improve the J_{sc}. So, no evident improvement of the J_{sc} and η can be seen between 20 bi-layers and 10 bi-layers GSCT films added DSSCs (more details see Supporting Information and Fig. S3). In fact, the J_{sc} and η are closely related with the dark current of the DSSCs. The dark current is resulted from the combination of electrons from the glass substrate and I_3^- ions, which makes the loss of photocurrent [35]. In order to further confirm the function of the transport layer, the dark currents of these samples were recorded (Fig. 5a). The values for the GSCT (10 bi-layers)-P25 photoanode based DSSCs are smaller than that of P25 photoanode based sample at the same potential above 0.56 V, and the onset of the dark current shifts to a higher potential (increase by 0.09 V) after adding the GSCT layer. Thereby, a lower combination rate between photogenerated electrons and I_3^- ions is achieved by using the GSCT-P25 photoanode. The fast electron separation and transport through the graphene network in the GSCT are the reasons for the reduced dark currents and increased J_{sc}. Moreover, the EIS was adopted to further study the carrier transport and interface property of the DSSCs with P25 and GSCT-P25 photoanodes (Fig. 5b). The Z' and Z'' axises are the real and imaginary parts of the impedance, respectively. There are two semicircles can be seen in the high-frequency and middle-frequency regions in both curves. The former reflects the impedance of the charge transfer process in the counter electrode, while the latter is related to the charge transport process at the photoanode–electrolyte interface [36]. Compared to that of the DSSC with the P25 photoanode, the semicircle size in the middle-frequency of the GSCT modified sample obvious decreases, suggesting the acceleration of the electron transport process and the decrease of photogenerated electron loss (combination of electrons from the glass substrate and I_3^- ions from the electrolyte) between conductive glass and electrolyte [19]. Therefore, the additional GSCT layer improves the interface property of the DSSC. Furthermore, the lamellar structure of the GSCT film is particularly appropriate for the ion transport, which further increases the J_{sc}. In order to make full use of the transport layer, 10 bi-layers GSCT film is a proper choice to be added into the photoanode (6.46% for η).

Similarly, the addition of GTNTs film improves the J_{sc} evidently as well. Compared to that of the pure P25 photoanode with same

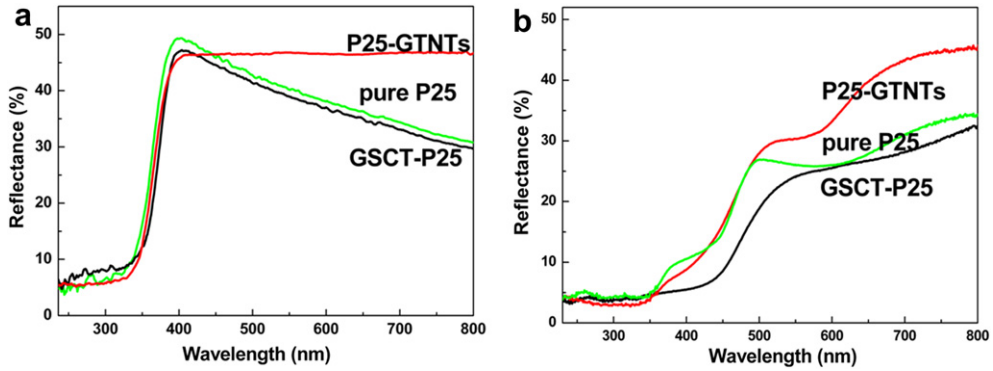

Fig. 4. UV–vis diffuse reflectance spectra of the P25, GSCT-P25 and P25-GTNTs photoanodes (a) without dye loading; (b) with dye loading.

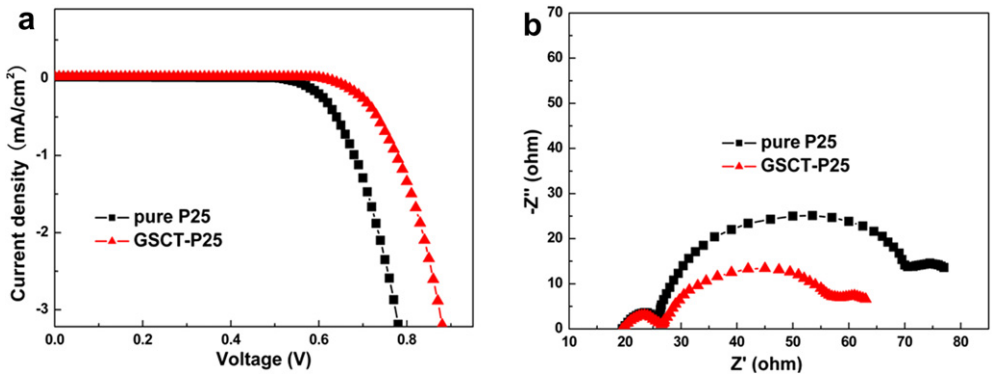

Fig. 5. (a) Dark currents and (b) EIS curves of the DSSCs with P25 and GSCT-P25 photoanodes.

thickness, the V_{oc} is also boosted by using the P25-GTNTs photoanode (Table 1). The large BET area ($\sim$300 m^2 g^{-1}) and mesoporous structure of the as-prepared GTNTs lead to an outstanding dye adsorption ability (see Table 1), which enable the DSSCs a better light response. Another reason for the upgraded photovoltaic properties is the ameliorative light utilization ratio due to the extra scattering layer. A distinguished scattering property of a photoanode is in favor of the light-harvesting efficiency as well as the high energy conversion efficiency. P25, as a commercial product, possesses nice absorption property and relatively low recombination rate of the electron–hole pairs, but suffers from a drawback of the low light-harvesting efficiency due to the size of the particles ($\sim$40 nm). Therefore, adding a GTNTs film that consists of particles with several hundred nanometers scale is a useful method to enhance the light-harvesting efficiency. The diffused reflection properties of the P25 and P25-GTNTs photoanodes were recorded, and the UV–vis diffuse reflectance spectra of them with and without dye absorption are shown in Fig. 4. Before dye absorption, the similar reflectivity of the two samples can be found in the range of 230–400 nm. In the long wavelength region, the reflectivity of P25 photoanode decreases rapidly. Contrarily, the parameter of the P25-GTNTs photoanode maintains a high level. The high reflectivity of the latter indicates the better light-harvesting ability, which can be attributed to the comparable size of the GTNTs particle and the wavelength of visible light [37]. The SEM images of the P25 and GTNTs (1 wt% graphene) are shown as Fig. 6, and evident difference in the particle size can be seen. After dye absorption, the reflectivities of all samples decrease significantly in the long wavelength region due to the light absorption by dye molecules. However, the P25-GTNTs photoanode possesses higher reflectivity than that of P25 photoanode, demonstrating the outstanding light scattering properties of the GTNTs layer. Consequently, the evident increases of J_{sc} and V_{oc} of the P25-GTNTs photoanodes based DSSCs also originate from their excellent scatter properties. It is worth noting that although GTNTs films contain graphene, they do not touch the conductive glass directly. Hence the graphene in the GTNTs cannot play as the electron transport channel. The amount of graphene in the GTNTs seems to give a slight influence on the photovoltaic properties of the DSSCs. The optimum results can be achieved when the mass fraction of graphene is 1 wt%. The potential reason is suggested as following: the presence of graphene can restrain the excessive assembly of the TNTs and make the particles with a proper size (see Fig. S4). However, the black graphene absorbs visible-light to interact with phonons (raising temperature) [38,39]. With the increased amount of graphene, the colors of the GTNTs change from white for pure TNTs to light grey for GTNTs with 1wt% graphene, and further change to dark brown for 10 wt% graphene contained GTNTs (see Fig. S5). Accordingly, the η increases to 7.54% for the P25-GTNTs (1 wt% graphene) based DSSC from 6.25% for the pure P25 based one, and then decreased to 6.92% for the P25-GTNTs (10 wt% graphene) based sample.

The IPCE curves of the DSSCs with varied photoanodes provide further evidence to confirm the functions of the transport and scattering layers (inset of Fig. 7). An increase in the IPCE over the entire wavelength range is obtained for the GSCT (10 bi-layers)-P25 photoanode based DSSCs, in which the electron separation and transport are more effective than that of P25 photoanode (better electrical property). Due to the superior optical property and large BET area, the excellent light scattering and dye absorption abilities of the P25-GTNTs photoanode improve the IPCE, as well. The obvious enhancement appears in the long wavelength range (from 550 nm to 700 nm in the absorption tail), which is attributed to the

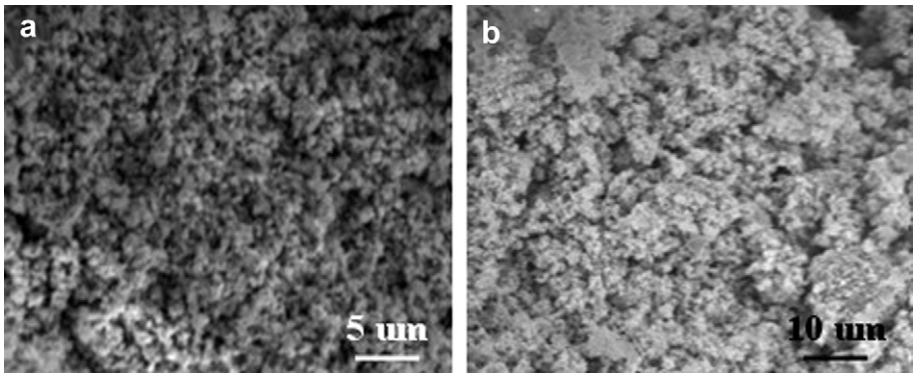

Fig. 6. SEM images of the P25 and GTNTs.

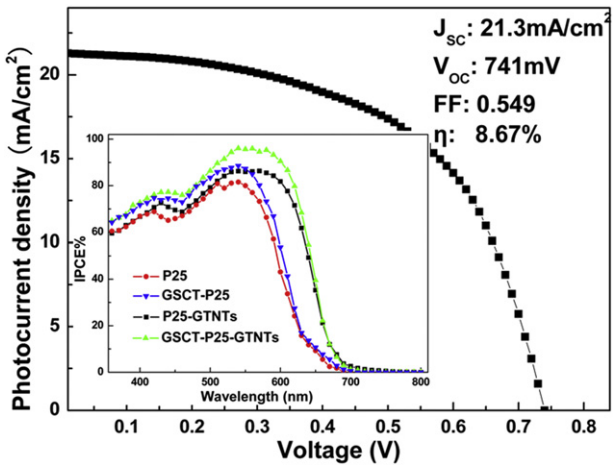

Fig. 7. *J–V* curve of a preliminarily optimized DSSC based on the GSCT-P25-GTNTs photoanode under AM-1.5G one sun intensity, the inset displays the IPCE curves of the DSSCs with P25, GSCT-P25, P25-GTNTs and GSCT-P25-GTNTs photoanodes.

comparable size between the GTNTs particles and the wavelength of incident light.

Based on above analysis and comparison, we can see that the excellent light-harvesting properties and large BET area of the scatting layer and outstanding electrical property and loosened layered structure of the transport layer lead to the higher η of the as-prepared DSSCs. Naturally, the GSCT-P25-GTNTs photoanode is anticipated to further improve the photovoltaic property of the DSSCs. After preliminary optimization the photoanode structure, a η as high as 8.67% is obtained. Thereinto, 10 bi-layers GSCT film and 1 wt% graphene contented GTNTs film are used as the transport and scattering layers, respectively. Compared to 6.25% for the pure P25 photoanode based DSSCs (15 μm), the excellent synergetic effect between the GSCT (~22 nm), P25 (10 μm) and GTNTs (5 μm) layers leads to the significant increase of the photovoltaic properties. Fig. 7 shows the *J–V* curve of the resulted DSSC, where the J_{sc}, V_{oc}, FF (filling factor) are 21.3 mA cm^{-1}, 741 mV and 0.549, respectively. The further improvement can be achieved by adjusting the thickness and constituents of these layers. In addition, adding graphene in the work layer with a proper amount can produce further enhancement for the η [11,40]. A η exceeding 9% is gained after adding 5 wt% graphene into the P25 layer (Fig. S6). The further work on optimizing the photoanode structure is under research.

4. Conclusions

In this work, GSCT and GTNTs films are fabricated and used as adding layers in the photoanode to improve the photovoltaic properties of DSSCs. The excellent electrical property of the GSCT film promotes fast electron transport and inhibits the recombination of electron–hole pairs. The similar scale between wavelength of incident light and particles in the GTNTs films endows the photoanode with higher light scattering efficiency, which improves the light response of the DSSCs. Moreover, large BET area of the GTNTs and loosened lamellar structure of the GSCT enhance the dye absorption and ion transport abilities, and hence further improve the J_{sc} and η. Compared to that of a pristine P25 photoanode based DSSC, the conversion efficiency for the GSCT-P25 and P25-GTNTs photoanode based DSSCs increase 33.8% and 20.6% in this study, respectively. After preliminary optimization the GSCT-P25-GTNTs photoanode, a η as high as 8.67% is obtained.

Acknowledgements

This work was supported by the National Natural Science Foundation of China (51076094, 51176113). The authors thank Instrumental Analysis Center of SJTU for FTIR measurement.

Appendix A. Supplementary material

Supplementary data related to this article can be found in the online version at http://dx.doi.org/10.1016/j.jpowsour.2012.07.093.

References

[1] B. Oregan, M. Gratzel, Nature 353 (1991) 737.
[2] M.K. Nazeeruddin, P. Pechy, T. Renouard, S.M. Zakeeruddin, R.H. Baker, M. Gra1tzel, J. Am. Chem. Soc. 123 (2001) 1613.
[3] M.K. Nazeeruddin, P. Pechy, M. Gratzel, Chem. Commun. 33 (1997) 1705.
[4] T. Horiuchi, H. Miura, S. Uchida, Chem. Commun. 39 (2003) 3036.
[5] W. Xu, J. Pei, J.F. Shi, S.J. Peng, J. Chen, J. Power Sources 183 (2002) 792.
[6] J. Rochford, D. Chu, A. Hagfeldt, J. Am. Chem. Soc. 129 (2007) 4655.
[7] G.D. Sharma, P. Suresh, M.S. Roy, J.A. Mikroyannidis, J. Power Sources 195 (2010) 3011.
[8] E. Stathatos, P. Lianos, A. Laschewsky, Chem. Mater. 13 (2001) 3888.
[9] Q. Wang, W. Campbell, E. Bonfantani, J. Phys. Chem. B 109 (2005) 15397.
[10] C.Y. Lin, Y.H. Lai, H.W. Chen, J.G. Chen, C.W. Kung, R. Vittal, Energy Environ. Sci. 4 (2011) 3448.
[11] P. Brown, K. Takechi, P.V. Kamat, J. Phys. Chem. C 112 (2008) 4776.
[12] K.M. Kiran, Z. Yong, Y.L. Yan, P.L. Kian, Adv. Funct. Mater. 19 (2009) 3638.
[13] X. Wu, Q.G. Li, L.Z. Wang, Energy Environ. Sci. 4 (2011) 3565.
[14] N. Balis, T. Makris, V. Dracopoulos, T. Stergiopoulos, P. Lianos, J. Power Sources 203 (2012) 302.
[15] J.G. Yu, J.J. Fan, B. Cheng, J. Power Sources 196 (2011) 7891.
[16] W.K. Tu, C.J. Lin, A. Chatterjee, G.H. Shiau, S.H. Chien, J. Power Sources 203 (2012) 297.
[17] K.S. Novoselov, A.K. Geim, S.V. Morozov, D. Jiang, Y. Zhang, S.V. Dubonos, I.V. Grigorieva, A.A. Firsov, Science 306 (2004) 666.
[18] X. Wang, L. Zhi, K. Mullen, Nano Lett. 8 (2008) 323.
[19] S.R. Sun, L. Gao, Y.Q. Liu, Appl. Phys. Lett. 96 (2010) 083113.
[20] Q.Q. Zhai, B. Tang, G.X. Hu, J. Hazar. Mater. 198 (2011) 78.
[21] F. Yang, Y.Q. Liu, L. Gao, J. Sun, J. Phys. Chem. C 114 (2010) 22085.
[22] T. Sasaki, Y. Ebina, T. Tanaka, M. Harada, M. Watanabe, Chem. Mater. 13 (2001) 4661.
[23] T. Sasaki, S. Nakano, S. Yamauchi, M. Watanabe, Chem. Mater. 9 (1997) 602.
[24] W. Lv, F. Sun, D.M. Tang, H.T. Fang, C. Liu, Q.H. Yang, H.M. Cheng, J. Mater. Chem. 21 (2011) 9014.
[25] B. Tang, G.X. Hu, H.Y. Gao, Appl. Spectrosc. Rev. 45 (2010) 369.
[26] H. Zhang, X.J. Lv, Y.M. Li, Y. Wang, J.H. Li, ACS Nano 4 (2010) 380.
[27] P. Lian, X.F. Zhu, S.Z. Liang, Z. Li, W.S. Yang, H.H. Wang, Electrochim. Acta 55 (2010) 3909.
[28] S. Takayoshi, W. Mamoru, J. Am. Chem. Soc. 120 (1998) 4682.
[29] Z.G. Wang, Y.F. Chen, P.J. Li, X. Hao, J.B. Liu, R. Huang, Y.R. Li, ACS Nano 5 (2011) 7149.
[30] S.M. Peak, E.J. Yoo, I. Honma, Nano Lett. 9 (2009) 72.
[31] B. Seger, P.V. Kamat, J. Phys. Chem. C 113 (2009) 7990.
[32] Y.J. Zhang, T. Mori, L. Niu, J.H. Ye, Energy Environ. Sci. 4 (2011) 4517.
[33] Y. Li, W.N. Wang, Z.L. Zhan, M. Woo, C.Y. Wu, P. Biswas, Appl. Catal. B Environ. 100 (2010) 386.
[34] T.Y. Wu, M. Tsao, F.L. Chen, S. Su, C.W. Chang, H.P. Wang, Y.C. Lin, W. Yang, W. Sun, Int. J. Mol. Sci. 11 (2010) 329.
[35] S. Ito, P. Liska, P. Comte, R.L. Charvet, P. Pechy, U. Bach, S.M. Zakeeruddin, A. Kay, M.K. Nazzerruddin, M. Gratezel, Chem. Commun. 41 (2005) 4351.
[36] H. Choi, H. Kim, S. Hwang, Y. Han, M. Jeon, J. Mater. Chem. 21 (2011) 7548.
[37] S. Hore, C. Vetter, R. Kern, H. Smit, A. Hinsch, Sol. Energy Mater. Sol. Cell 90 (2006) 1176.
[38] L.W. Zhang, H.B. Fu, Y.F. Zhu, Adv. Funct. Mater. 18 (2008) 2180.
[39] J.S. Park, S.M. Cho, W. Kim, J. Park, P.J. Yoo, Appl. Mater. Interfaces 3 (2011) 360.
[40] T.H. Tsai, S.C. Chiou, S.M. Chen, Int. J. Electrochem. Sci. 6 (2011) 3333.